TBIRD, a rapid prototyping approach for design, assembly, and test of a LEO-to-ground lasercom CubeSat

Noah C. Gilbert, Bryan C. Bilyeu, Joshua J. Brown, Jesse S. Chang, David R. Crompton, Ajay S. Garg, Andrew J. Horvath, Lawrence J. Petrilli, Robert S. Reeve, Kathleen M. Riesing, Bryan S. Robinson, Curt M. Schieler, Miyoung P. Schue, Joseph J. Scozzafava, Jade P. Wang

MIT Lincoln Lab, 244 Wood Street, Lexington, United States

ABSTRACT

The TeraByte InfraRed Delivery (TBIRD) system is a 3U payload on a 6U CubeSat launched in May 2022 which has now demonstrated space to ground links of >1 Terabyte (TB) per pass at a max data rate of 200Gbps. As a CubeSat mission, the development of the TBIRD payload was focused on low SWaP and a "rapid prototyping" approach which accepted higher risks to accelerate the schedule and reduce costs. The optomechanical design process followed standard in-house processes to develop a system that would be robust to LEO environmental loads, with a focus on the stability of the transmit (Tx) and receive (Rx) channel performance metrics. The driving requirement of maintaining 20µrad pointing error between the TX and Rx channels forced specific attention to thermal and mechanical load changes over operational conditions, which drove major design decisions. This paper describes some of engineering challenges overcome and approaches used to make TBIRD a successful program, as well as some of the tradeoffs of rapid prototyping precision optical payloads. TBIRD successfully met and exceeded the total downlink requirements listed above, with a bandwidth of 200Gbps and a total downlink of 4.8TB of information in a single pass.

1. INTRODUCTION

The TBIRD mission is a 3U payload manifested on a 6U CubeSat host bus as part of the NASA Pathfinder Technology Demonstration (PTD) missions to demonstrate a new optical communications system architecture that can deliver terabytes of data per day from a CubeSat in LEO orbit.[1−3] The TBIRD payload is designed to utilize commercial telecommunications transceivers to achieve high burst rates up to 200Gpbs from LEO to ground. The low-rate uplink is used for retransmission requests to provide error free communications, and additionally provides pointing feedback to the host spacecraft.

The program is a rapid development effort, with an aggressive schedule focused on making a rideshare launch, and complementary higher risk acceptance compared standard space mission. This paper describes the design considerations and build aspects for the free-space optical monolith that functions as the interface between the internal modem and the remote terminal. In order to achieve the target downlink rates of 200Gbps and single pass transfers larger than 1TB over the entire operational environment a significant amount of engineering effort was focused on the stability of the optomechanical design. The initial design intent was to produce a system that could downlink to a 40cm aperture ground station with a nominal TX full-width-half-max (FWHM) divergence of 109µrads. The design and build of the flight unit had a timeline of two years, with a focus on the rapid development and deployment of a space based payload with posture of high risk tolerance.

2. DESIGN CONCEPT

Lasercom terminals typically follow one of two design paradigms, combining the uplink and downlink beams internally and using a common launch aperture, and a bi-static system with separate apertures per the receive (Rx) and transmit (Tx) channels. The size, weight, and power (SWaP) limitations for TBIRD required judicious use of space for the free-space optical system, the 3U allotted to the payload also contains the modem and payload electronics. We were able to leverage

DISTRIBUTION STATEMENT A. Approved for public release. Distribution is unlimited. This material is based upon work supported by the National Aeronautics and Space Administration under Air Force Contract No. FA8702-15-D-0001. Any opinions, findings, conclusions or recommendations expressed in this material are those of the author(s) and do not necessarily reflect the views of the National Aeronautics and Space Administration.

legacy system designs to close a few design trades early: fiber ferrule bonded to a Tx launch using a glass donut, lenses epoxied in place, and a quad cell as the Rx detector. Specification for design consideration as listed in Table 1 were used as the baseline for the optical design.

Table 1. TBIRD Derived Optical Specifications

Specification	Value
Full Field of View (Rx)	±0.25°
Tracking Field of View (Rx)	±500µrads
Offset Tracking (Tx to Rx)	±75µrads
Bus open-loop pointing	±0.25°
Far Field Divergence (Tx)	<130µrads FWHM
Boresight Static (Tx to Rx)	<150µrads
Boresight Dynamic (Tx to Rx)	<100µrads
Throughput Loss (Tx,Rx)	<1dB
Aperture (Rx)	2.3cm

2.1. Design Architecture Trades

For larger aperture systems a common aperture design is favored due to the relaxation of optical alignment requirements of the back end optics given the magnification of the common front end telescope. A major drawback of sharing a single aperture between the uplink and downlink channels is the requirement to have channel isolation on the order of 90dB. In a common aperture setup, the channel isolation relies on dichroic filters with bandpass transition requirements that are very steep, this often requires significant engineering effort on the coatings that drive up the unit cost. Magnification in a common telescope of 15x would produce a beam size that is 1.06mm $1/e^2$ diameter, which starts to become an issue for power density at filters and scattering from surface roughness. For a bi-static design the channel isolation is automatic, there is an aperture per channel. Separation of channels removed the need to have exquisite filters to do the stray light mitigation. The major risk with a bi-static approach is the potential for boresight drift between the Rx and Tx channels, both as single post-launch shift and also for dynamic pointing shifts over the environmental range during operation due to self-heating. To combat the risk of relative boresight drift a bi-static design was formed around an optical monolith, with the minimum number of interfaces between the optics and the supporting structure. Figure 1 describes the layout of the components in the bi-static design that was used for TBIRD.

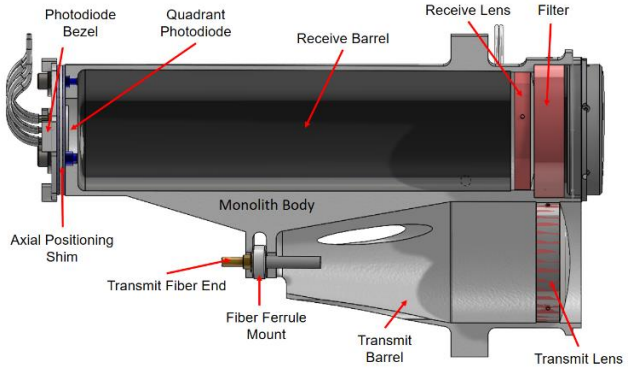

Figure 1. TBIRD Bi-static optical monolith side view with components labeled, reprinted from [4]

2.2. Optical Requirements

TBIRD is a bus pointed lasercom terminal, and with that comes an uncertainty in the ability of the payload host bus to respond to the payload's commands accurately. The optical design incorporates the pointing knowledge error of the host bus, which was assumed to have a 3σ pointing error of 85µrads. Divergence of the Tx beam was nominally set to 110µrads FWHM at 1560nm, with a range of 110µrads to 130µrads allowed for a 1dB of signal loss at a 40cm diameter aperture remote terminal due to wavefront error.

$$\Theta = \frac{\sqrt{2}FWHM}{\sqrt{ln2}} \quad (1)$$

$$\Theta = \frac{2\lambda}{\pi\omega_0} \quad (2)$$

$$f = \frac{\emptyset}{NA} \quad (3)$$

Where ω_0 is the radial beam waist, λ is the wavelength, NA is the numerical aperture of the fiber, and ∅ is the diffraction limited beam diameter, and f is the effective focal length (EFL) . Combining (1) and (2) as an input to (3) the nominal focal length given a FWHM of 110µrads is 57.6mm. It was decided to have a longer EFL of 58mm to allow the beam to spoil slightly due to incurred WFE and maintain the design far field FWHM divergence.

Use of a quad cell as the Rx channel detector sets two fields of view for the system, one for the field of view for the entire sensor, and one for the common response region (discriminant) based on the size of the point spread function as seen by all four quadrants of the quad cell. The full field of view of the quad cell where the defocused spot is fully on the sensor is ±0.25° as shown in Figure 2 as the payload acquisition range. The linear response region is used to perform fine tracking during optical communication with the remote terminal, and incorporates all static and dynamic pointing offsets. The nominal size of the tracking field of view is ±500µrads, which maps directly to region where the point spread function (PSF) is on all four quadrants at the same time. The active area of the quad cell is 1mm in diameter, using $h = f\ tan\ \theta$ with θ = 0.25° and h = 0.5mm the nominal focal length is 114.6mm. The proportional response region of ±500µrads translates to ±0.029°, and using the previous equation with $\theta = 0.25° + 0.029° = 0.279°$ the EFL becomes 102.3mm. This was rounded to 100mm to add margin for quad placement. With the 100mm EFL Rx lens a spot with a ±500µrad discriminant required a defocus of approximately 0.437mm.

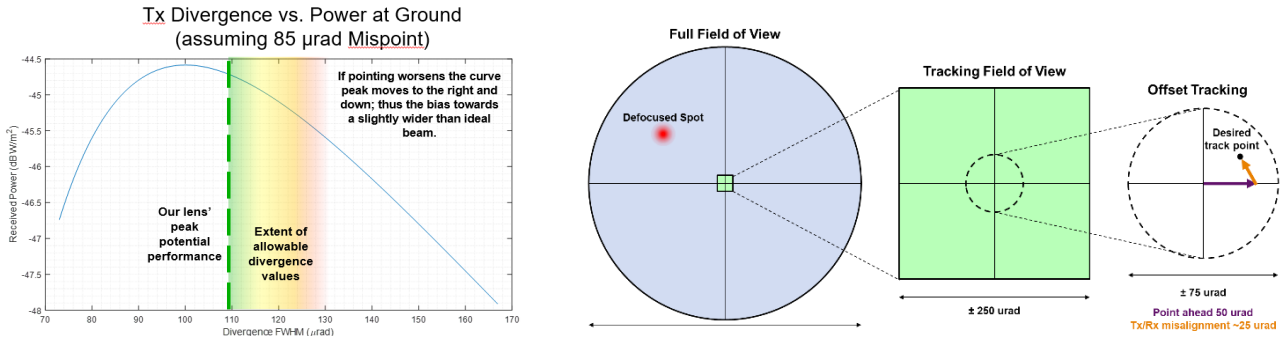

Figure 2. (Left) Received power at remote terminal vs. aperture, (Right) Rx tracking modes with field of view [4]

2.3. Environmental Considerations

The LEO orbit chosen has an average distance of 500 km. The thermal limits for the payload as modeled are -15°C and +25°C for the cold and hot operational modes respectively. The TBIRD payload uses a burst communication paradigm [1], which results in self-heating due to thermal isolation from the host bus when fully powered on and transmitting during a pass. The pass length is on the order of several minutes, which means all of the operational modes are outside of a thermal soak case. The optical monolith is required to survive a thermal range of -15°C to +50°C, during which the survival heaters maintain the thermal range. The LEO radiation environment at 500 km does not present significant risk

to glass photodarkening. At this lower LEO elevation one of the major drivers for optical damage is corrosion from atomic oxygen, and our materials and coatings took this into account.

2.4. Design for LEO Environment

In order to meet the system performance across the expected thermal environment a passively athermal design was chosen. Thermal analysis was run on the payload in the space entrainment to generate the operational and survival ranges for the system, the details of this analysis are outside the scope of this paper. The output from the thermal analysis is an expected operational for the optical monolith of 0°C to +25°C, and a survival range of -15°C to +50°C. To minimize the shift in focus over the operational thermal range both the glass and metering structure were chosen according to their combined therm-optic coefficient and CTE [4].

$$\beta = \alpha_g - \frac{1}{n-1}\frac{dn}{dT} \tag{4}$$

The change of focal length for a refractive optic in air [4] is given as

$$\Delta f = f(\beta - \alpha_c)\Delta T \tag{5}$$

Where β is the therm-optic coefficient, dn/dT is the thermal coefficient of the lens refractive index, n is room temperature index of refraction of the lens, and α_g is the glass CTE. The defocus term Δf change in focus from the nominal room temperature focus position, which is a function of β, the change in temperature ΔT, and the CTE of the metering structure holding the lens, with the assumption that this is a radially bonded lens. The combination of a less than two year lifetime and the LEO radiation environment allowed for the use of non-radiation hard glasses. This provided significant relief in the opto-mechanical design space, where expanding the glass choice will better balance CTE mismatch and changes in focus vs temperature. Using equations (1) and (2) it was possible to create a table of materials that contained their thermally induced focus shift and CTE.

From Table 2 it is clear that there are few options for matching thermal power and CTE for Aluminum, given the closest glass CTE has a delta of 10ppm/°C. There are CTE matches to 416 and 420 stainless steel and titanium within ±1ppm/°C range, which is our target for smaller athermalized bond gaps. Titanium was chosen for the lower density and potential SWaP savings in terms of mass. A drawback is that it has a lower thermal conductivity compared to stainless steel, which requires the optical monolith be thermally isolated from the payload structure to reduce thermal gradients. Reduction in bond gap size reduces the available motion of the optics over the thermal range.

$$t_B = r_O \frac{(1-\nu_B)(\alpha_C-\alpha_O)\}}{\alpha_B-\alpha_C+\nu_B(\alpha_B-\alpha_O)} \tag{6}$$

Equation (6) [5] was used to determine the optimized bond gap given the glass, bond material, and housing CTE values $[\alpha_G, \alpha_B, \alpha_C]$as well as the bond material's Poisson ratio ν_B.

Table 2. Table of glass thermal power coefficients, CTE, and availability

Glass	Thermal Power	CTE	Status/Type
N-LAK21	6.2	6.8	Preferred
N-LAK7	7.3	7.1	Preferred
N-LAK12	9.65	7.6	Preferred
N-LAF2	8.53	8.06	Preferred
N-SF11	8.84	8.52	Preferred
Titanium	8.6	8.6	Metal
SFL57	9.09	8.7	Special
P-SF69	8.44	8.99	Preferred
SFL6	10.65	9	Special

N-SF6	10.44	9.03	Preferred
N-SF6HT	10.44	9.03	Preferred
N-SF6HTULTRA	10.44	9.03	Preferred
LF5	8.11	9.1	Preferred
LF5HTI	8.11	9.1	Preferred
N-SF10	10.55	9.4	Preferred
P-SF8	10.21	9.41	Preferred
N-SF4	10.78	9.45	Preferred
N-KF9	8.04	9.61	Preferred
Stainless 416	9.9	9.9	Metal
Stainless 420	10.3	10.3	Metal
ULTRAN30	23.83	11.9	Structural
N-FK51A	25.11	12.74	Preferred
P-PK53	24.16	13.31	Special
Aluminum	23	23	Metal

2.5. Lens Tolerancing

The design choice of a bi-static optical system comes with the requirement that both static and dynamic offsets are within a recovery region defined by the Tx divergence and the Rx field of view. The static boresight difference between the channels needed to be less than 150µrads radially, with an allocation of up to an additional 100µrads for the dynamic drift post launch and over thermal excursions during operation. The Tx lens design is diffraction limited to a defocus of ±50µm, which results in ~0.37 waves PV, 0.10 waves RMS, with power being the major contributor. Reserving 0.25 waves PV for the dynamic errors and margin, the lens can have up to 0.2 waves PV, which is achieved with a specification of 0.5 fringes at 633nm per surface. The wavefront change for the Tx lens over a 40°C thermal swing has a range 0.0036 waves PV, and 0.0004 wave RMS at 1560 nm of has shown in Figure 3 . This variation is below the expected wavefront measurement to measurement error and well within the design budget. Manufacturing tolerances shown in Table 3 were set via Monte Carlo analysis to produce lens where the Tx fiber was allowed to move within the mechanical constraints of the fiber ferrule mount to correct for focus and other aberrations while maintaining a PV WFE under 1/20 waves at 1560nm . The metric for the Rx lens is change in the discriminant width defined as the region where the PSF is measured on all four quadrants of the quad simultaneously. Discriminant width is nominally ±500µrads, with a tolerance of ±20µrads. An allocation of 0.15° of wedge in the part allows for an additional 0.5° of mounting error with only 14µrads change in the discriminant as estimated using a line spread function [Figure 3].

Table 3. Lens tolerances

Radius	3 fringe	at 633 nm
Irregularity	0.5 fringe	at 633 nm
Thickness	0.15	mm
Outer Diameter	+0.000/-0.010	mm
Index	±5e-4	unitless
Abbe	0.5	percent
Wedge	<0.010	mm over diameter

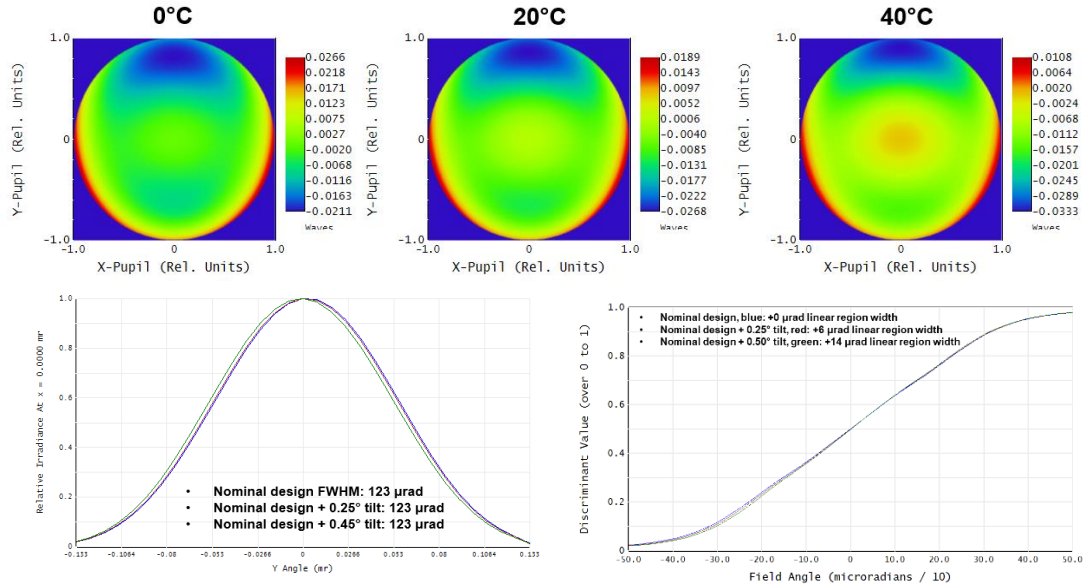

Figure 3. (Top) Tx lens Monte-Carlo wavefront results (Middle) Tx lens thermal wavefront performance over a 40°C range (Bottom) Tx lens tilt divergence sensitivity, Rx lens tilt discriminant sensitivity

3. ASSEMBLY AND INTEGRATION

The build cycle of the TBIRD monolith presented a change to the general approach to precision optical systems in regards to the number sequential operations that are final. The two lenses, the spectral filter, and the fiber are all bonded directly to the monolith, which creates four operations where deviations from nominal conditions could require the entire assembly to be scrapped. As the TBIRD program was envisioned as an experiment in rapid development for a higher risk CubeSat payload, the traditional approach of an engineering development unit (EDU), Qual and flight development was eschewed for a rapid direct-to-flight build. In addition, the optical test set was designed and built to be a simplified test set that would target key measurements without requiring substantial investment in budget at time.

3.1. Lens Alignment

The optical monolith does not have any lips or seats for the lenses, all bonds are direct to the inner wall of the respective lens tubes. Direct glass to housing bonds were chosen to reduce the amount any single element could shift due to stress relaxation in the epoxy when going through thermal excursions. Both the Tx and Rx lenes have metering flats as rear surfaces, these flats were used to set the tilt of the optics relative to the monolith lens barrels. From our tolerance analysis in Section 2, it is shown that tilt tolerance of the Tx lens allows for 0.5° tilt to maintain the allotted wavefront error of $WFE \leq \lambda/20$, and accordingly the Rx lens has the same tolerance. To meet the alignment requirement of 0.5° degrees tilt of the lenses with respect to the housing a fixture was designed to mount the optical monolith vertically, which allowed precision double side polished flats (wedge < 1 arcmin) to be loaded onto support pillars and viewed with an alignment telescope for a live alignment to the mechanical housing.

Using multiple precision flats, it is possible to view the angle of the monolith housing, the Rx pedestal and the Tx pedestal with an alignment telescope. There were two pillar designs given the layout of the monolith and the Tx fiber mount preventing a simple pedestal as was used with the Rx channel as seen in Figure 4. To align the Tx to the optical monolith the three support pillars were all adjustable, and they were adjusted with the precision flat installed until the observed return on the alignment telescope was within the required 0.5° with respect to the housing.

3.2. Lens Bonding

The alignment pillars set the height and angle of the lens with respect to the housing, and both the Tx and Rx lenses were shimmed to center prior to bonding. The initial bond design was a full annular bond line to prevent any asymmetry in the

bond pads from causing lens drift during thermal changes. Multiple test bonds were performed with a surrogate bond fixture, and the results showed that in order to achieve an annular bond the epoxy would first flow above and below the lens and encroach onto the optical surfaces. To keep the process simple and reduce risk to the optics from cleaning epoxy or epoxy wrapping around the edges and creating areas of significant stress we determined that symmetric bond pads would be sufficient. An added boon for going with a pad bonding method is that the centering shims can remain installed during the entire bond process to prevent and shifting during the epoxy cure. Each lens was bonded individually, with a thermal cycle between the alignment and bonding steps per lens as a check for any gross bond problems.

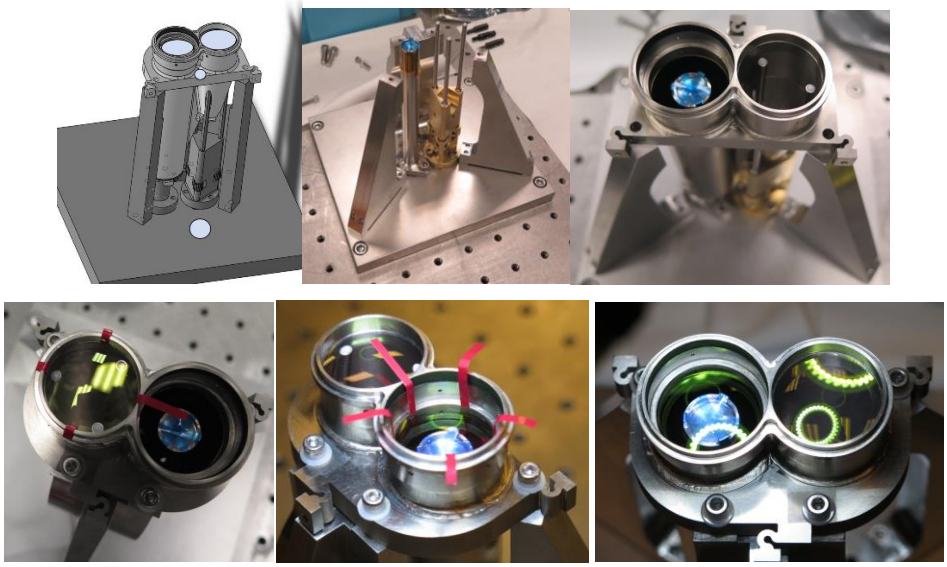

Figure 4. (Top, Left to Right) Precision flat locations, alignment fixture before loading, monolith installed on fixture (Bottom, Left to Right) Tx lens installed, Rx lens installed, Rx and Tx lenses bonded

3.3. Filter Assembly

The spectral isolation filter had the most lenient alignment tolerance, where system performance was met over a tilt range of ±3° shown in Figure 5. This allowed the filter to be mounted into a separate retaining bezel via a clamping ring with shims between the metal and glass. The use of shims allowed for a larger CTE mismatch between the filter substrate material and the titanium housing. As a separate assembly it was also possible to thermal cycle the populated filter bezel to check for workmanship problems before attaching it to the monolith. The filter bezel seat was machined to the same tolerances of the Rx and Tx bores, where a perpendicularity tolerance of 0.002” over 1.131” results in a max angular error of 0.10°.

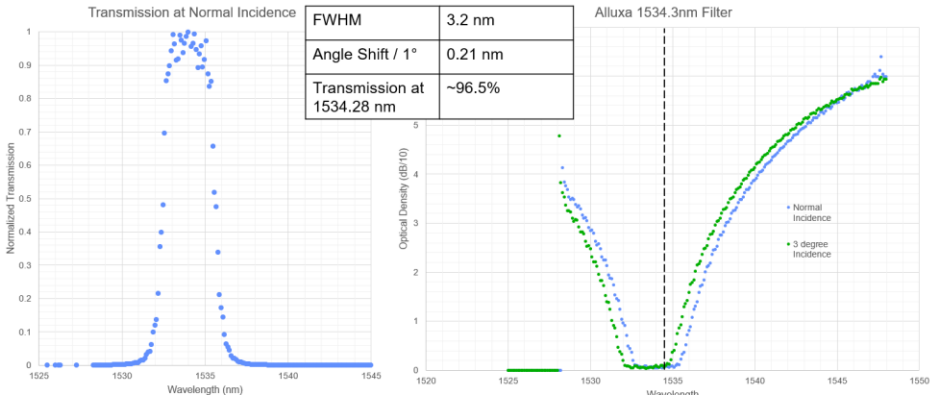

Figure 5. Rx spectral filter performance vs alignment

3.4. Build Testbed Setup

The testbed built for TBIRD needed to measure the far field divergence of the Tx beam, scan a beam over the ±0.25° field of view of the Rx channel, and measure the relative pointing between Tx and Rx channels. Due to metrology equipment availability multiple one time use configurations were used prior to the system test configuration. A wavefront sensor was used to collimate a 50.8mm diameter 750mm focal length lens to provide a input beam that had less than 5% intensity roll-off over the lens clear aperture. The Rx discriminant is sensitive to the intensity distribution of the input beam, with the on-orbit use case being presented a nominally flat intensity profile over the 23mm Rx clear aperture. Testing the Rx over the entire field required scanning a fast steering mirror (FSM) that was observed with an autocollimator as pointing feedback. To maintain the beam position on the Rx aperture a 1:1 relay was used to map the FSM aperture and RX aperture to pupil planes Figure 6. For boresight the spatial separation of the Tx and Rx channels was used to split the beam paths in height along the optical table. To co-boresight the source for the Rx channel a corner cube retroreflector was placed in the Rx beam with an offset from the center point of the cube to shift the return beam into the Tx boresight camera with a nominal static pointing error < 15µrads.

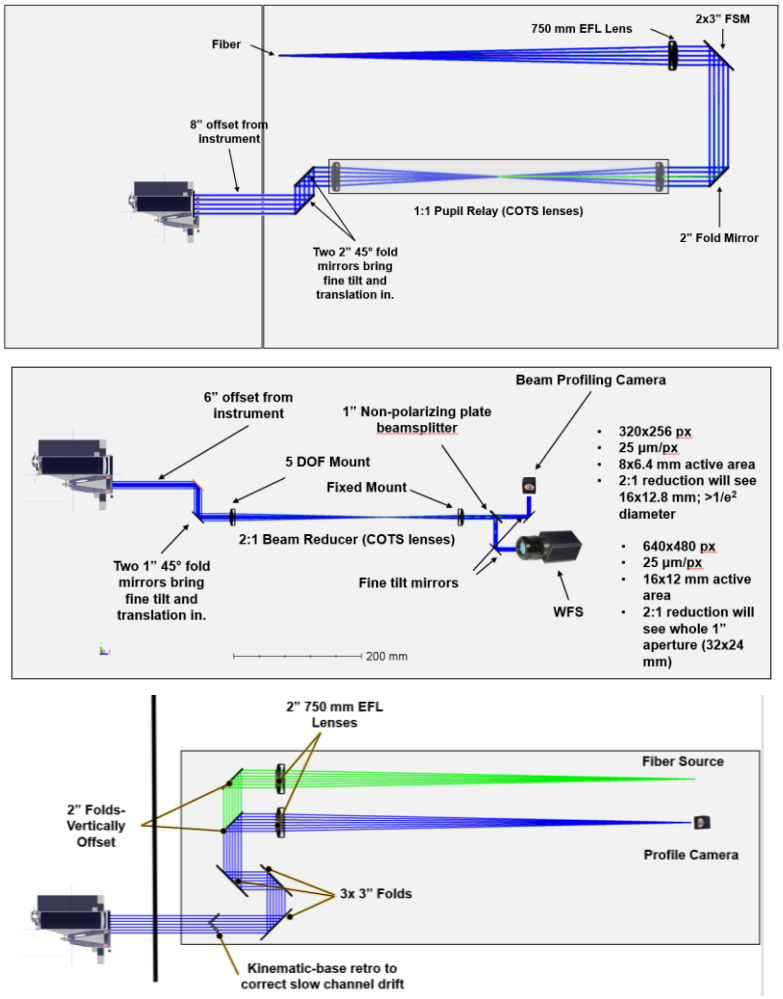

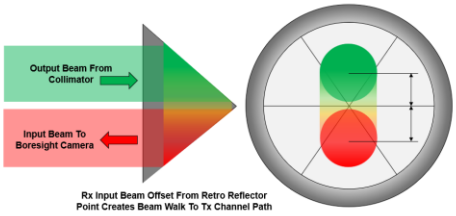

Figure 6. (Top to Bottom) Rx alignment configuration, Tx fiber alignment configuration, channel boresight configuration, boresight calibration retroreflector detail

3.5. Tx Channel Alignment

TBIRD uses an angled fiber ferrule as the modem to free-space interface, which was aligned using a wavefront sensor to minimize wavefront error. The ferrule is held with a 5 axis stage to allow for translation and pointing adjustment while observing the wavefront error when the Tx output is on. The wavefront error of the Tx is measured live while the fiber ferrule is adjusted, with the ferrule aligned without the glass disk that ultimately bonds the fiber to the housing to allow for less restrictive motion of the fiber. When the wavefront was measured to be below 0.08 waves PV at 1550nm the position of the stage micrometers is noted and the ferrule is lifted out to allow the glass disk to be installed. The stage is them moved back to the recorded position, with small adjustments to re-optimized the wavefront measurement. With the wavefront requirement met the disk and ferrule were bonded to the monolith housing. Post bonding the divergence was measured on a camera at a pupil relay to calculate the FWHM before and after thermal cycling the unit as shown in Table 3.

Table 3. Pre and post thermal cycling Tx performance

Test	FWHM Divergence	PV WFE at 1560nm	RMS WFE at 1560nm
Baseline	124.1µrads	0.072	0.012
Post Thermal Cycle	126.7µrads	0.072	0.015

3.6. Rx Channel Alignment

Alignment of the Rx channel is accomplished by aligning the quad cell to be co-boresighted to the output Tx beam. The designed discriminant is ±500µrads, with the uncalibrated zero point as the intersection of the four active detection areas. During the first pass at rough alignment it became clear that there was a problem with how far off nominal the quad cell needed to be translated to bring the center of the quad to the relative alignment of the Tx. The total adjustable range of the Rx quad is ±0.5°, and while closing in on the centration we reached the mechanical limit of translation. On review of the Tx fiber position, it became evident that the reported wavefront error had been insufficient to place the output beam along a range capturable with the quad cell as designed. Lack of a pointing reference during the Tx alignment due to the specific testbed configuration needed allowed the Tx fiber ferrule to be bonded in a position that was reporting good wavefront error and missed the range of pointing correction. This was noted as an oversight and a requirement for any future testbed layouts.

There were several options available to correct this error, ranging from debonding the fiber to starting over with a new monolith. As part of the rapid approach TBIRD took with the build the decision was made to use the existing monolith as-built. The easiest and lowest risk to correct for the pointing error was to add a wedge and correct the error optically. The offset angle was measured to be approximately 1.1° using pictures of the Tx fiber ferrule and measured distances to the mechanical housing, which was easily accommodated by a COTS wedge.

Using a COTS allowed for a near complete correction of the pointing offset that did not present risk to the existing hardware. To correct for the approximate 1.1° pointing offset a 2° wedge was chosen as the beam deviation is nominally 1°. Mechanically we had some additional volume in the payload envelope in front of the optical monolith to allow for the addition of a mounted wedge. The same bonding approach as the lenses was used to bond the lens to a titanium bezel. The

inside bore on the fore of the Rx channel was painted with black paint to reduce specular stray on the quad cell, and could not be part of a structural bond. This forced the use of a face bond to mount the wedge bezel. The wedge housing required a 0.002" bond gap with an area coverage greater than 30% to meet the margin required for launch loads. A mockup of aluminum and plexiglass was used to develop the bond process, as the required geometry for the bond would cause any excess epoxy to flow down onto the Rx filter. Squeeze out of the epoxy droplets was a concern, which was mitigated by producing epoxy beads that created zero squeeze out when using a 0.002" bond wire as seen in Figure 7. With the wedge installed a final set of test data was taken before the monolith was ready for integration into the payload. Pre-housing integration data is shown in Table 4.

Table 4. Assembled Optical Monolith Performance

Parameter	Requirement	Measured
Full Field of View (Rx)	±0.25°	±0.29°
Tracking Field of View (Rx)	±500µrads	±450µrads
Far Field Divergence (Tx)	<130µrads FWHM	126.7 µrads FWHM
Boresight Static (Tx to Rx)	<150µrads	20.88µrads Y, 6.41µrads Z

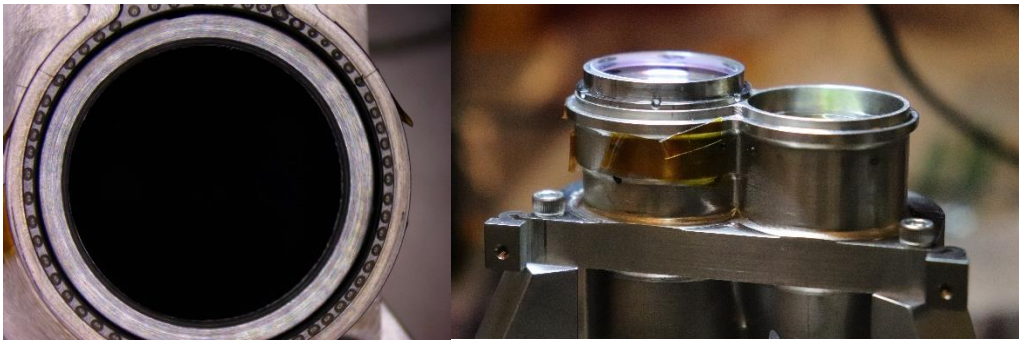

Figure 7. (Left) Rx channel housing with epoxy applied (Right) Rx wedge bonded

4. TEST

All of the individual channel testing was done in preparation for system level testing with the optical monolith installed into the flight payload. Payload environmental testing includes in-air ambient testing pre and post vibration, as well as functional testing at all nominal operating temperatures in a vacuum chamber. The build testbed was laid out on two parts of ½ inch breadboard plate on top of a larger 2 inch honeycomb breadboard. Separating the two ½ inch plates into a unit under test (UUT) section and the metrology section allowed the metrology section to be portable. For the TVAC test campaign the build testbed was relocated to the TVAC chamber. As a testbed validation measurement the integrated system was tested on the Optical Terminal Verification Testbed (OTVT) to compliment the build testbed data with metrology that was impossible to obtain with a single simplified TBIRD build testbed configuration. Measurements on OTVT were intended to bookend the vibration tests, as test durations were short enough to be completed in the downtime between major OTVT test campaigns. To ensure appropriate operation in the space environment, proto-flight testing was done on the CubeSat payload. Environmental testing included vibration testing as well as thermal-vacuum testing, and a final end-to-end validation of performance. For vibration testing, we validated the boresight and wavefront were identical (within the error of measurement) prior and post shake to ensure no mechanical concerns. For Thermal-Vacuum testing, we measured various optical metrics while the payload was in vacuum and confirm performance in the expected environment. For brevity, this paper address key data points in the test campaign, and the ensuing analysis to determine payload viability.

4.1. Payload Ambient Baseline Testing

The payload was populated with the optical monolith, changing the previous test source to the flight Tx laser and the temporary Rx quad electronics to the flight electronics and field programmable gate array (FPGA). First pass testing was done on the optical build discriminant test set, and the monolith close out testing was re-run to evaluate for changes post payload integration.

The next step prior to vibration testing was to compare the TBIRD build testbed results to OTVT. The test aperture on OTVT is variable, with a stepped set of aperture sizes. The best fit for a single channel would be the 1" aperture, but with the need to fill both Tx and Rx apertures simultaneously with a single aperture we went with the 2" aperture. . OTVT relays a scaled pupil internal to the testbed to the aperture of the unit under test (UUT), which allows for testing field without beam translation at the UUT aperture. The scaled aperture on OTVT has a calibration method and tracked scale factors for both the wide and narrow field of view cameras to map pixel instantaneous field of view (IFOV) to far field angle space for the UUT. Alignment of the TBIRD payload to OTVT involved identifying the relayed pupil position in free-space using a SWIR camera and a mechanical aperture mask. The payload was aligned to the physical mask such that the space between the two apertures was centered in the OTVT pupil mask.

Boresight error was measured as the difference between the centroid of the beam for the OTVT source and the TBIRD Tx output on the NFOV camera when the TBIRD Rx quad showed a calibrated equal response from all 4 active quad cell active areas. Alignment to the Rx quad was achieved by adjusting the OTVT steering mirror and monitoring the TBIRD Rx quad output. The corresponding Tx to Rx boresight on OTVT was 15.72µrands in Y and 20.95 µurads in Z. Once aligned to the testbed a discriminant fun was performed by scanning the OTVT FSM across the active range of the TBIRD Rx quad. The timeframe for this test was limited, the thermal design for TBIRD utilizes a frustrated thermal path from the structure to the optical monolith for conduction, but in the presence of air that was overcome by convection from the hot electronic parts. Noise on the Rx quad becomes significant as the unit self-heats, limiting operation to <30min tests. Discriminant values measured on OTVT showed a range of ±170µrads, which was approximately a factor of 2 smaller than the previous testbed measurements or ±450µrads. The narrow field of view (NFOV) camera used for boresighting has a calibrated IFOV scale, and the focused Tx spot was used for a scaled far field divergence measurement. Fitting the 2D gaussian intensity profile resulted in far field divergence value of 498microradians. Wavefront measurement of the Tx beam on OTVT was possible with the caveat that ratio of the Tx aperture to the 4" OTVT projected pupil resulted in a 4x reduction of sampled points on the OTVT wavefront sensor. The wavefront data showed what is largely focus error with 0.73 waves PV, 0.146 waves RMS. These deviations in divergence and discriminant kicked off an investigation of both testbeds, as retesting the payload produced the same results on each respective testbed.

4.2. Testbed Investigation

Disentangling the two datasets sparked an examination of the build testbed. Comparative testing started with a search for a second method for validating the wavefront of the source collimator. A sheer plate and an additional camera were made available to support the test, and immediately bore fruit. The collimator produced approximately 2 waves of focus over the 2" aperture as viewed with the shear plate and the SWIR camera. The same collimator was then tested against the wavefront sensor that had been initially used to setup the testbed, which reported wavefront error of less than 0.1 waves PV. In order to rule out a faulty calibration file in the wavefront sensor as a static bias, the collimator was adjusted to produce no perceivable fringes and tested again. The now well aligned collimator produced similar wavefront numbers on the wavefront sensor, confirming that there was more than a static bias from the existing reference file. Since this wavefront sensor had been used for all of the build testbed alignments, as well as the Tx wavefront measurement, all measurements on the build testbed were suspect.

Fortunately, by this time a different and recently calibrated wavefront sensor had become available for our use. The sensor format for the new wavefront sensor was smaller, 9mm x12mm. The change in sensor format required a 2:1 beam reducer to be designed to capture the 16mm Tx output beam. The 2:1 beam reducer was setup as a Keplarian telescope and aligned using a Fizeau interferometer in double pass with a single pass transmitted WFE< 0.01 waves RMS at 1550nm. An iris at the intermediate focus allowed the relay to be placed into the system and aligned to the corrected field angle quickly,

opening the iris to find the beam when the input angle was incorrect and narrowing it down to maintain alignment to the well corrected field angle.

4.3. Continued Testing

Maintaining schedule and the reservation of the shaker table required shake and shock test during the testbed investigation. The basis for this decision was that the differences between the two testbeds were a function of the testbeds, and self-consistent. This allowed vibration testing to happen during the investigation, as both testbeds could still be used to make relative measurements to evaluate changes from vibration. Shake and shock testing are significant mechanical tests and will not be covered in detail in this paper. Standard practice is to measure the performance of the system prior to shake and shock testing and post testing to compare relative performance.

Table 5. OTVT data for TBIRD payload performance before and after shake

	FWHM X	FWHM Y	FWHM AVG	Boresight Z,Y	Tracking Field
Prior to Shake	453µrads	529µrasd	491µrads	4.4µrads, 3.3µrads	±270µrads
After Shake	443µrads	515µrads	479µrads	-8.2µrads, -5.2µrads	±270µrads

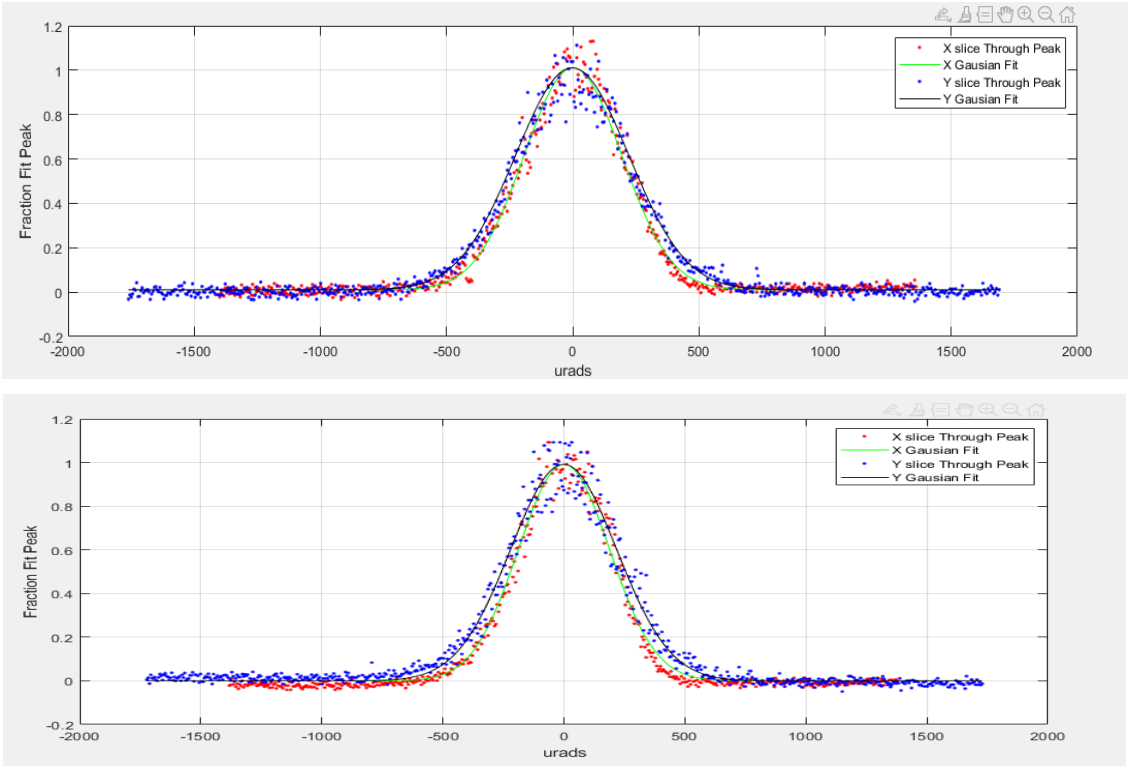

Figure 8. Overlaid NFOV cross sections in X and Y through far field spot peak, normalized. Top Pre-shake, Bottom Post-shake

4.4. Thermal Vacuum (TVAC) Testing

Measuring the payload operation in vacuum was a significant program milestone and a critical performance data point. The payload was loaded into a bell jar using a soft conforming thermal pad to create a compliant interface for the non-flight GSE used to hold the unit during TVAT testing. The bell jar used has an existing optical output window designed to impart negligible wavefront error in the C-band for testing lasercom terminals over their operating thermal ranges while

under vacuum. The build-testbed with the wavefront corrected collimator and new WFS with 2:1 relay was moved and setup in front of the output window for metrology. Measurements of the wavefront error, boresight, and discriminant were measured at the following points: in-air in chamber, post pump-down, hot operational, cold operational, nominal operational. Tracking the changes of the payload performance across the operational thermal range became paramount to the system operation as the reduction in the discriminant range limits the previous static and dynamic boresight shift allocations. Some margin had been bought back during the Rx alignment, where the static offset was limited to under 25µrads radially where there was an initial allocation of 150 µrads.

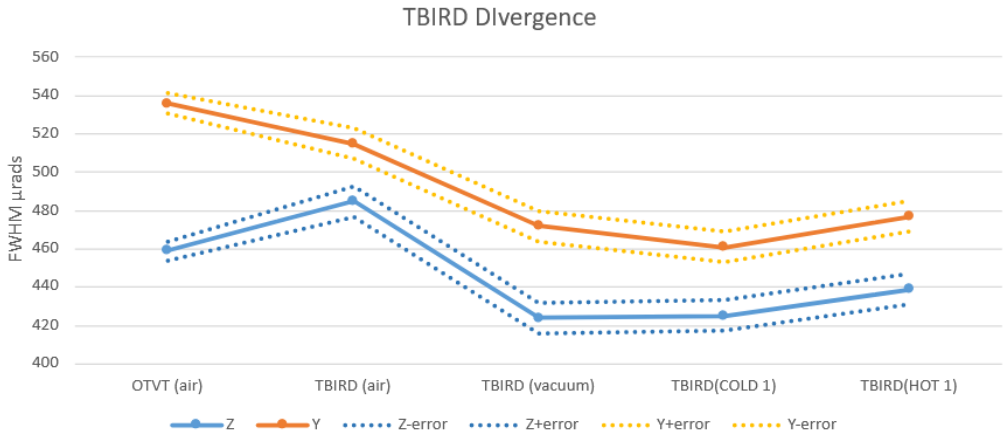

Figure 9. TBIRD Divergence variation during TVAC testing

4.5. On-Orbit Results

The TBIRD payload successfully launched in May 2022 as part of NASA's PTD series. The spacecraft first detected the uplink signal on Jun 11th, and the downlink was first detector on June 24th the same year. The TBIRD mission utilized the NASA Optical Communications Telescope Laboratory (OCTL) at NASA JPL Table Mountain in southern California. The OCTL telescope has a 1m aperture [5], presenting more signal gain than the 0.4m aperture that the system was designed for. This increased diameter quadrupled the collection area of the aperture, counteracting most of the increased energy loss due the much higher Tx divergence. On orbit data reprinted from [6][7].

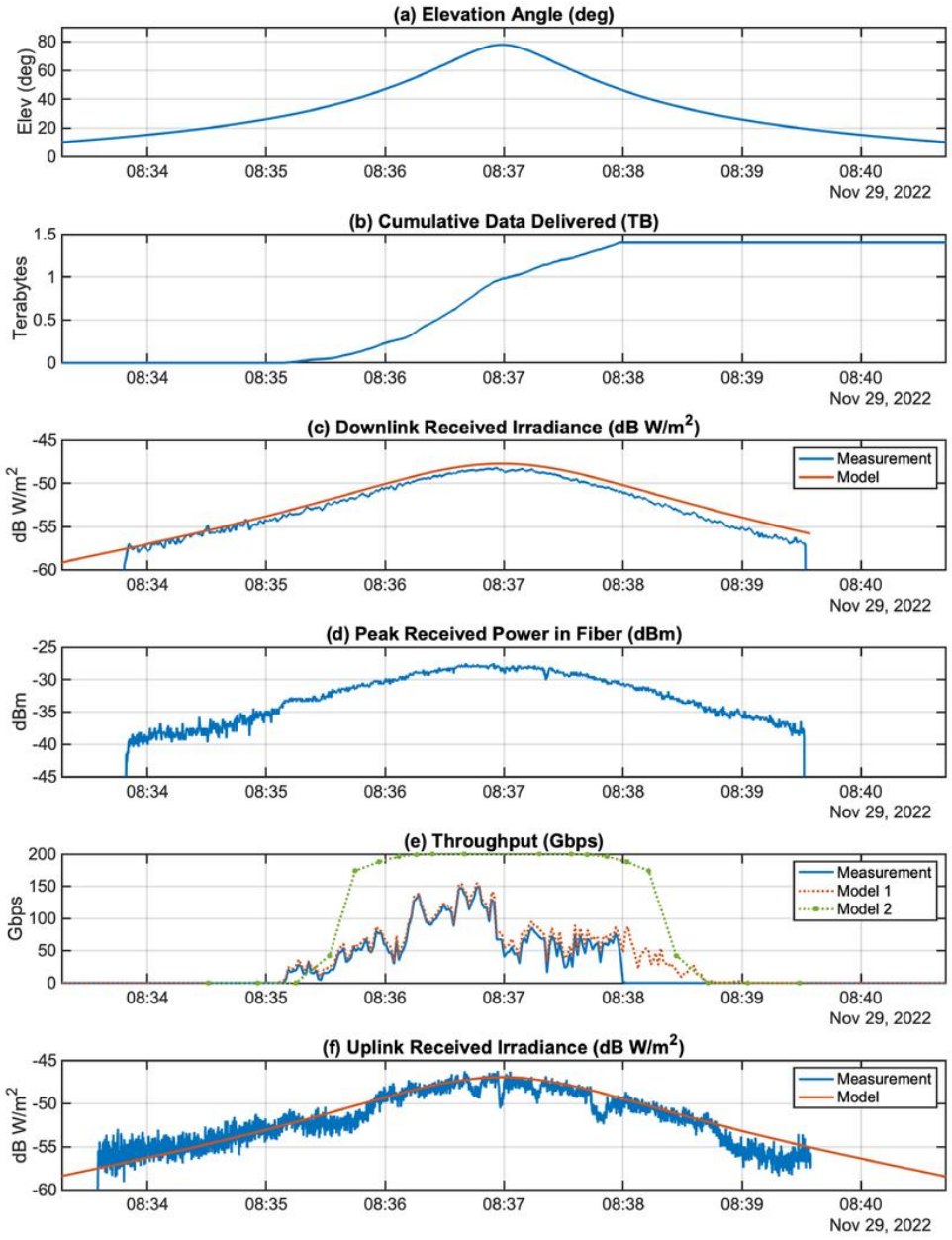

Figure 10. Telemetry and performance results from a TBIRD pass. Time axes are in UTC. Initial uplink detection occurred at 12° elevation. (b) The downlink operated in 200-Gbps mode and transferred 1.4 Terabytes error-free. (c) The downlink irradiance was stable throughout the pass as the closed-loop body pointing system tracked the uplink. (d) The peak envelope of the received power in fiber, calculated by post-processing the 25 kSam/s raw timeseries and then taking the maximum power achieved in each 200-ms interval. (e) The throughput, calculated with 1-s averaging, reached 150 Gbps during the pass. (f) The uplink irradiance received by space terminal was stable and provided the tracking signal and an error-free ARQ uplink feedback channel [6]

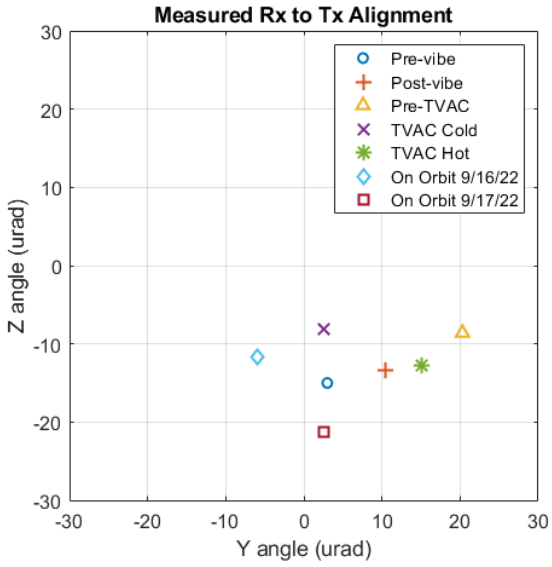

Figure 11. Measurements of transmit to receive boresight before and after launch. The mean Tx/Rx misalignment is 15 µrad with a standard deviation of 10 µrad. [7]

5. CONCLUSION

The TBIRD mission was a success, the payload on-orbit performance demonstrated COTS lasercom components in the LEO environment using 200Gbps burst transmission to downlink over 1TB in s single pass. The program's rapid approach on delivering a flight payload eschewing an EDU, coupled with the monolithic optical design presented unique challenges to execution of the build phase of the program. The largest single hurdle for the optical build became the validation of the testbed, which was an ongoing issue during the entire build process. Discovery of the faulty wavefront sensor post during environmental testing presented a turning point in the build flow, with a re-evaluation of the optical performance and the payload viability. Maintaining a live system budget with incorporation of measured component performance to payload performance was critical to quickly overcoming the issues encountered during the build. It was extremely fortunate that the magnitude of the divergence and discriminant departures from nominal were recoverable through the engineering efforts initially placed on minimizing boresight drift and active boresight alignment during the build process. Team communication and cohesiveness allowed the program to overcome the challenges encountered and supply a payload that met the mission requirements to schedule and within budget. As of the writing of this paper the TBIRD payload has demonstrated a single pass downlink of 4.8TB.

ACKNOWLEDGEMENTS

The research described in this publication was in part carried out by the Jet Propulsion Laboratory, California Institute of Technology, under a contract with the National Aeronautics and Space Administration.

REFERENCES

[1] Robinson, B., Boroson, D., Schieler, C., Khatri, F., Guldner, O., Constantine, S., Shih, T., Burnside, J., Bilyeu, B., Hakimi, F., et al., "TeraByte InfraRed Delivery (TBIRD): a demonstration of large-volume direct-to-Earth data transfer

from low-Earth orbit," in [Free-Space Laser Communication and Atmospheric Propagation XXX], 10524, 105240V, International Society for Optics and Photonics (2018).

[2] Schieler, C., Robinson, B., Guldner, O., Bilyeu, B., Garg, A., Riesing, K., Chang, J., Hakimi, F., Brown, J., Khatri, F., et al., "NASA's terabyte infrared delivery (TBIRD) program: Large-volume data transfer from LEO," AIAA/USU Conference on Small Satellites (2019).

[3] Schieler, C. M., Garg, A. S., Bilyeu, B. C., Wang, J. P., and Robinson, B. S., "Demonstration of reliable high-rate optical communication over an atmospheric link using arq," in [2019 IEEE International Conference on Space Optical Systems and Applications (ICSOS)], 1–6 (2019).

[4] Katie Schwertz, Dan Dillon, and Scott Sparrold "Graphically selecting optical components and housing material for color correction and passive athermalization", Proc. SPIE 8486, Current Developments in Lens Design and Optical Engineering XIII, 84860E (11 October 2012); https://doi.org/10.1117/12.930968

[5] Piazzolla, S. et al., "Ground station for terabyte infrared delivery (TBIRD) ," in [Free-Space Laser Communications XXXV], 12413, SPIE (2023).

[5] Daniel Vukobratovich, Ken A. Fetterhoff, James R. Myers, Paul D. Wheelwright, George R. Cunnington, "Bonded mounts for small cryogenic optics," Proc. SPIE 4131, Infrared Spaceborne Remote Sensing VIII, (16 November 2000); https://doi.org/10.1117/12.406545

[6] Curt M. Schieler, Kathleen M. Riesing, Bryan C. Bilyeu, Jesse S. Chang, Ajay S. Garg, Noah J. Gilbert, Andrew J. Horvath, Robert S. Reeve, Bryan S. Robinson, Jade P. Wang, Sabino Piazzolla, W. Tom Roberts, Joseph M. Kovalik, Beth Keer, "On-orbit demonstration of 200-Gbps laser communication downlink from the TBIRD CubeSat," Proc. SPIE 12413, Free-Space Laser Communications XXXV, 1241302 (15 March 2023); https://doi.org/10.1117/12.2651297

[7] Kathleen M. Riesing, Curt M. Schieler, Jesse S. Chang, Noah J. Gilbert, Andrew J. Horvath, Robert S. Reeve, Bryan S. Robinson, Jade P. Wang, Paaras S. Agrawal, Robert A. Goodloe, "On-orbit results of pointing, acquisition, and tracking for the TBIRD CubeSat mission," Proc. SPIE 12413, Free-Space Laser Communications XXXV, 1241305 (15 March 2023); https://doi.org/10.1117/12.2651957